tvst

Retina

OCT Angiography of Type 1 Macular Neovascularization in AMD: A Morphometric Evaluation

Maria Cristina Savastano[1,2,*], Claudia Fossataro[2,*], Matteo Mario Carlà[2], Valentina Cestrone[1], Ilaria Biagini[1], Clara Rizzo[3], Raphael Kilian[3], Sandrine A. Zweifel[4], Daniel R. Muth[4], Francesco Faraldi[5], Stanislao Rizzo[1,2,6,7,], and David Sarraf[8,9,**]**

[1] Ophthalmology Unit, Fondazione Policlinico Universitario Agostino Gemelli, IRCCS, Rome, Italy
[2] Ophthalmology Unit, Catholic University of the Sacred Heart, Rome, Italy
[3] Ophthalmology Unit, University of Verona, Verona, Italy
[4] Department of Ophthalmology, University Hospital Zurich, University of Zurich, Zurich, Switzerland
[5] Department of Ophthalmology, Istituto Oftalmico di Torino, Torino, Italy
[6] Consiglio Nazionale delle Ricerche (CNR), Istituto di Neuroscienze, Pisa, Italy
[7] Vitreoretinal Surgery Unit, Fatebenefratelli Isola Tiberina Gemelli Isola Hospital, Catholic University "Sacro Cuore," Rome, Italy
[8] Stein Eye Institute, University of California Los Angeles, Los Angeles, California, USA
[9] VA Greater Los Angeles Healthcare System, Los Angeles, California, USA

Correspondence: David Sarraf, Retinal Disorders and Ophthalmic Genetics Division, Stein Eye Institute David Geffen School of Medicine at University of California Los Angeles, Los Angeles, CA 90095, USA. e-mail: dsarraf@ucla.edu

Received: June 24, 2024
Accepted: November 26, 2024
Published: February 24, 2025

Keywords: advanced exudative age-related macular degeneration; macular neovascularization; OCT angiography; imageJ; fiji

Citation: Savastano MC, Fossataro C, Carlà MM, Cestrone V, Biagini I, Rizzo C, Kilian R, Zweifel SA, Muth DR, Faraldi F, Rizzo S, Sarraf D. OCT angiography of type 1 macular neovascularization in AMD: A morphometric evaluation. Transl Vis Sci Technol. 2025;14(2):23, https://doi.org/10.1167/tvst.14.2.23

Purpose: To determine biomarkers of macular neovascularization (MNV) in neovascular age-related macular degeneration through the application of an automatic algorithm based optical coherence tomography angiography (OCTA) analysis.

Methods: In this retrospective, observational, single-center, cross-sectional study, patients with a diagnosis of age-related macular degeneration complicated by type 1 MNV were included. MNV was detected with OCTA and scans were analyzed with a qualitative and quantitative open-source image processing package. For each analyzed image, we automatically acquired the following data: Total MNV area, vessel area, vessel density (VD), total number of branches, total number of vascular junctions, mean vessel length, mean vessel diameter, fractal dimension (FD), junction density, and vessel tortuosity.

Results: The following morphological parameters revealed a significant negative correlation with best-corrected visual acuity: MNV area – Spearman $\rho = -0.309$ ($P = 0.002$); vessel area – Spearman $\rho = -0.315$ ($P = 0.002$); total number of vascular junctions – Spearman $\rho = -0.285$ ($P = 0.005$), and VL – Spearman $\rho = -0.304$ ($P = 0.003$). Immature MNV lesions were significantly associated with better vessel area than mature and hypermature lesions.

Conclusions: Several automated MNV-associated morphological parameters can correlate with the best-corrected visual acuity. Further studies are warranted to determine if these OCTA biomarkers can be applied to guide anti-vascular endothelial growth factor therapy and predict response to treatment.

Translational Relevance: The analysis of MNV biomarkers may have prognostic value in terms of visual function.

Introduction

Neovascular age-related macular degeneration (NVAMD) is characterized by aberrant blood vessels that proliferate from the choroid into the sub-retinal pigment epithelium or outer retinal spaces.[1] Macular neovascularization (MNV) sequelae include subretinal bleeding, fluid leakage and exudation, lipid deposition, fibrosis, or a combination of these harmful complications that can impair vision and harm photoreceptors.[2,3] Therefore, the accurate assessment of the

morphology of MNV may play a crucial role in monitoring disease progression and guiding treatment decisions.

Although optical coherence tomography angiography (OCTA) has proven to be a noninvasive and practical tool for the diagnosis of MNV, its efficacy to provide biomarkers of NV activity has fallen short.[4,5] Although various groups have correlated OCTA features of MNV with NV activity, the majority of these biomarker studies failed to show an association. OCT remains the most important tool to determine MNV activity and guide anti-vascular endothelial growth factor (VEGF) treatment decisions.[6–9]

In the setting of myopic choroidal neovascularization, however, NV membrane area and flow area represent reliable indicators of successful intravitreal anti-VEGF therapy.[10,11] The OCTA biomarkers referred to as vascular connections and vascular branching may be accurate OCTA biomarkers of response, effectively guiding anti-VEGF therapy for myopic choroidal neovascularization.[12] Indeed, Li et al.[13] created a single imaging protocol combining OCTA and vascular branching analysis to assess NV activity associated with myopic choroidal neovascularization.

In our study, we applied an upgraded version of ImageJ to measure several MNV characteristics from OCTA scans and correlated these biomarkers with vision.

Methods

This was a retrospective, observational, single-center, cross-sectional investigation including patients with NVAMD. The study was carried out at the Fondazione Policlinico Universitario Agostino Gemelli, IRCCS, in Rome, Italy, and included patients followed at this center from September 2021 to January 2023. The research was authorized by the Catholic University of the Sacred Heart Ethical Committee in Rome, Italy, and adhered to the principles of the Declaration of Helsinki. All study patients provided signed, informed consent.

All participants underwent comprehensive ophthalmic examination, which included measurement of the best-corrected visual acuity (BCVA) according to the Early Treatment Diabetic Retinopathy Study (ETDRS), slit-lamp biomicroscopy, dilated funduscopic examination, spectral domain OCT, and OCTA (Solix full-range OCT, Optovue Inc, Freemont, CA). All examinations were performed on the same date.

Inclusion criteria were patients older than 50 years and the identification of subfoveal type 1 MNV owing to NVAMD. MNV lesions were either treatment naïve or previously treated with anti-VEGF therapy.

Exclusion criteria included types 2 and 3 MNV and polypoidal choroidal vasculopathy, MNV with predominant fibrotic scarring (well-demarcated elevated mounds of yellowish white tissue),[14] a history of central serous chorioretinopathy, myopia greater than 3 diopters, myopic CNVs, complete retinal pigment epithelial and outer retinal atrophy, namely, (1) a region of signal hypertransmission of at least 250 µm in diameter, (2) a zone of retinal pigment epithelium attenuation or disruption of at least 250 µm in diameter, (3) overlying photoreceptor degeneration, and (4) all abovementioned signs in the absence of retinal pigment epithelium tear, involving the fovea, evidence of other retinal diseases or low-quality OCT or OCTA scans (<7/10) owing to motion artifact, lens opacity, or blinking.

OCTA Acquisition

The Solix full-range OCT (Optovue Inc), a new ultra-high-speed spectral domain device with an acquisition speed of 120,000 A-scans per second using a split spectrum amplitude-decorrelation angiography algorithm, was used to acquire OCT and OCTA images.

A 6.4 × 6.4 mm OCTA scan was captured and the outer retinal and the choriocapillaris segmentation slabs were used to detect the presence of MNV. The Solix AngioVue program (version 2019 V1.0.0.317; Optovue, Inc.) *custom* feature was then used for MNV manual segmentation, modifying the slab thickness and axial location, to highlight the full extent of the type 1 NV membrane with the clearest border and the least perilesional artifacts. Thus, the OCTA images were extracted and subjected to qualitative and quantitative analyses.

MNV Images Qualitative Assessment

Three expert ophthalmologists classified and graded each MNV according to one of the following categories, based on the OCTA morphology, as previously reported[15,16]:

1) Immature MNV: MNVs characterized by a small uniform capillary network or rosette-like lesions with small capillaries.
2) Mature MNV: MNVs characterized by a large dilated vascular network with definite vascular

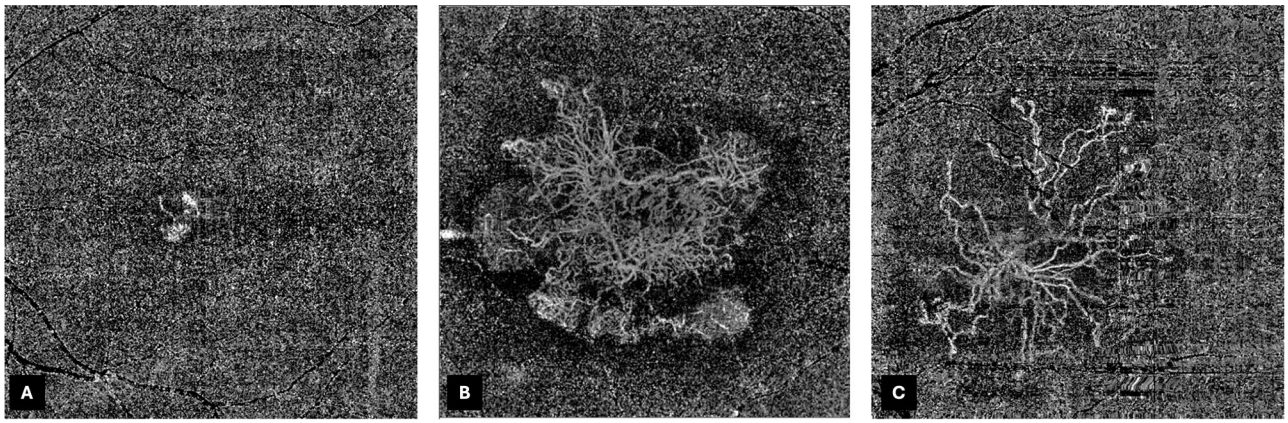

Figure 1. OCTA of immature, mature and hypermature MNV. OCTA showed immature MNV of few rosette with small, uniform capillaries (**A**), a mature MNV with large dilated vessels in a sea fan pattern and perilesional dark halo (**B**), and a hypermature MNV, characterized by long dilated filamentous straight vessels, with a "dead tree" aspect (**C**).

branching trunks typically organized in a sea fan aspect.

3) Hypermature MNV: MNVs with long and filamentous vessels, without intervening capillaries, anastomoses or vascular loops, with the typical presence of a visible main trunk.

See Figure 1 for representative OCTA examples of these three morphological grades.

MNV Images Quantitative Assessment

We used Fiji, an open source image processing package based on ImageJ2 that includes many useful plugins.[17] ImageJ is a powerful Java-based image processing program developed by the National Institutes of Health, specifically designed for image analysis tasks in biological sciences, as described in the existing literature.[18,19] Fiji's macro tool facilitates the automation of tasks and the addition of functionality to create forms, reports, and controls.

We used the macro tool described by Deshpande et al.,[20] which is based on an algorithm originally developed by Wang et al.,[12] to analyze OCTA pictures. First, we manually delineated the MNV using the built-in free-hand tool and deleted the outside area. Second, binarization was applied to all OCTA scans before quantitative analysis and a Gaussian kernel was used to denoise the MNV picture. The final binary OCTA picture was then created using a combined technique that included a Frangi Vesselness filter and local adaptive thresholding. Last, the macro tool automatically determined the total MNV area, the vessel area (VA) and the vessel density (VD) from the resulting image.

In a second passage, after applying the Mexican hat filter to the previously adjusted images, the lesions were skeletonized successively with automated main trunk and branch recognition. The skeletonized image was then analyzed to automatically determine the following quantitative morphological biomarkers: total number of branches and vascular junctions, mean vessel length, mean vessel diameter, fractal dimension (FD), junction density (JD) and vessel tortuosity (VT).

A flow diagram of the Fiji macro pipeline is presented in Figure 2. The extracted morphological features are consistent with previous reports in the literature[11,12,20,21]: We observed and analyzed 10 morphological biomarkers:

1. MNV area (mm^2): The area of the NV lesion as calculated according to the manually outlined boundaries of the MNV, indicating the entire size of the lesion.
2. VA (mm^2): The area of the NV lesion as calculated by highlighting the actual tracing of the vessels comprising the MNV (that appear white on OCTA scans).
3. VD: A vascular biomarker defined as the ratio of the area occupied by vessels (i.e., VA) to the entire MNV lesion area.
4. MNV branches (n): A vascular biomarker calculated as the sum of all the vessel limbs on the skeletonized images.
5. Vessel length (mm): A vascular biomarker calculated as the sum of Euclidean distances between the pixels of all the vessels in the MNV lesion, indicating the total NV length.
6. Vessel junctions (n): A vascular biomarker defined as the number of points of vascular

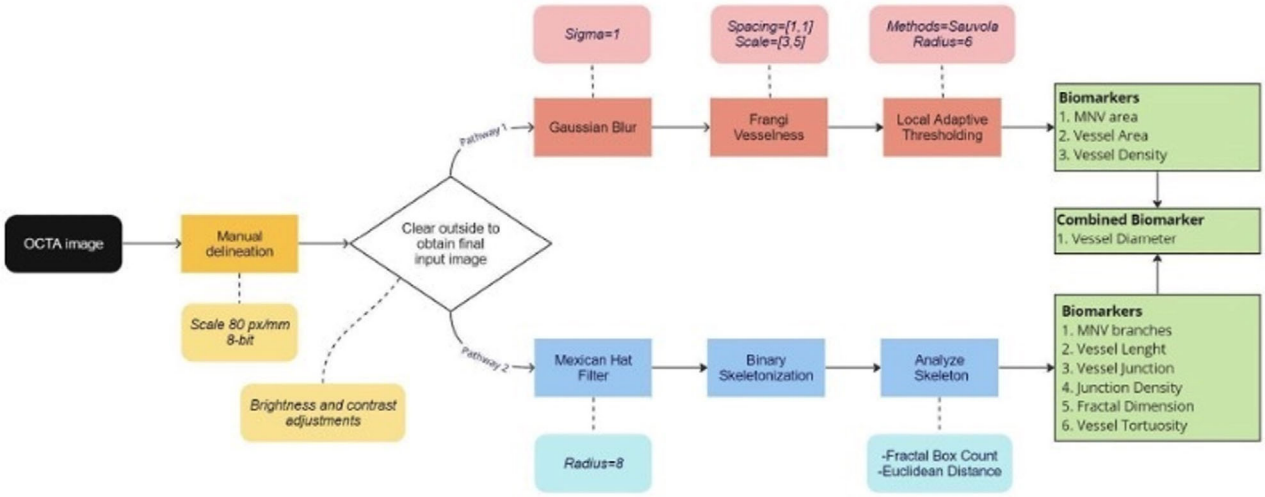

Figure 2. Image processing approach chart. Our algorithm uses manually cropped OCTA images for delineation and input. The next pipeline follows a double pathway structure. In pathway 1 (*upper way*), we denoise the image, applying the Gaussian blur, the Frangi filter, and local adaptive thresholding to measure area-related biomarkers including MNV area, VA, and VD. In pathway 2 (*lower way*), we apply the Mexican Hat filter and Binary Skeletonization to measure vascular biomarkers like total MNV branches (TMB), vessel length (VL), total number of vascular junctions, JD, fractal dimension (FD), and VT.

connection, indicating internal branching in the MNV network.

7. Vessel diameter ($\mu m^2/\mu m$): A vascular biomarker calculated as the ratio between nonskeletonized VA and skeletonized total vessel length, indicating the average vessel caliber of the MNV.
8. JD (n/mm): A vascular biomarker, defined as the ratio between the number of junctions and the total NV length. This refers to the anastomotic activity in proportion to the total NV length and reflects the activity of the MNV.
9. Fractal dimension: A numerical indicator of vessel branching complexity, obtained from the skeletonized binary image with the appliance of the box-counting method. Higher fractal dimension values indicate a more complex vessel branching pattern.
10. VT: A morphological biomarker that quantifies the microtortuosity of the MNV. It is calculated as the actual length of each branch divided by the imaginary straight length between two branch nodes.[18] Smaller tortuosity values indicate straighter vessels.

Statistical Analysis

Statistical analysis was conducted using GraphPad PRISM Software, (Version 9.5; GraphPad, La Jolla, CA). First, we performed a descriptive analysis of all data. Our sample's normality was determined using the Shapiro-Wilk test, and a *P* value of greater than 0.05 was used to confirm the null hypothesis. In those cases when our analysis violated these analysis of variance preconditions, we applied the Kruskal–Wallis test. In a post hoc analysis of the Kruskal–Wallis test, the uncorrected Dunn's test was performed for comparisons among subgroups, and *P* values were adjusted using the Bonferroni comparison. In addition, correlation studies were performed on continuous variables, and a binary logistic regression analysis was performed to assess the influence of OCTA biomarkers on visual outcomes. The quantitative results were reported as means and standard deviation, a *P* value of less than 0.05 was deemed statistically significant and the 95% confidence interval of the mean was adopted.

Results

One hundred twenty-seven eyes of 104 patients were included in this analysis. The mean age of the total cohort was 76.0 ± 5.8 years and male/female and right eye/left eye ratios were 45/59 and 66/61, respectively. The mean reported BCVA at the time of OCTA scan acquisition was 38.0 ± 27.9 letters (20/200). Twenty-one out of 127 eyes (16.5%) were treatment naïve and 106 eyes (83.4%) received previously other IVI.

Algorithm Performance

We tested the macro on a dataset of 127 manually cropped, expert-labeled OCTA images. We used the macro tool proposed by Deshpande et al.[20] to skele-

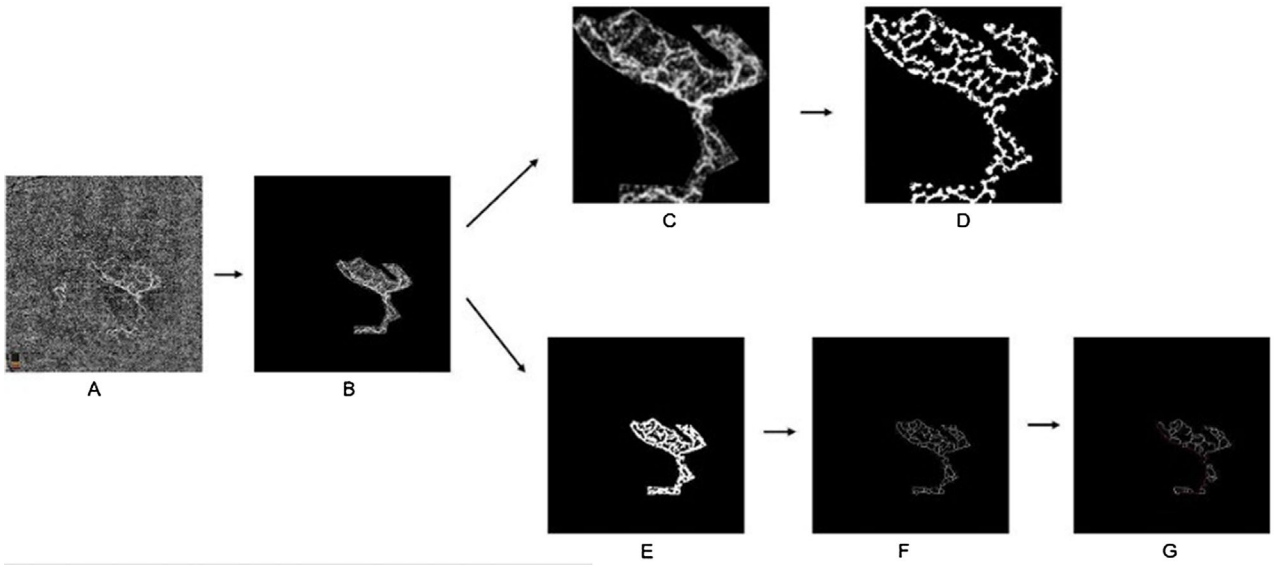

Figure 3. Intermediate stages of OCTA image processing during different pipeline phase in a case of naïve MNV. (**A**) Input OCTA image showing the active MNV lesion. (**B**) Manually delineated OCTA image. Upper pathway. (**C**) The Gaussian adjustment used for smoothing and denoising. (**D**) The Frangi vesselness filter applied to calculate MNV area, VA, and VD. Lower Pathway. (**E**) Binary skeletonization of the OCTA image using ImageJ. (**F** and **G**) The skeletonization was used to calculate the JD, vessel diameter (MVD), tortuosity (VT), and fractal dimension (FD).

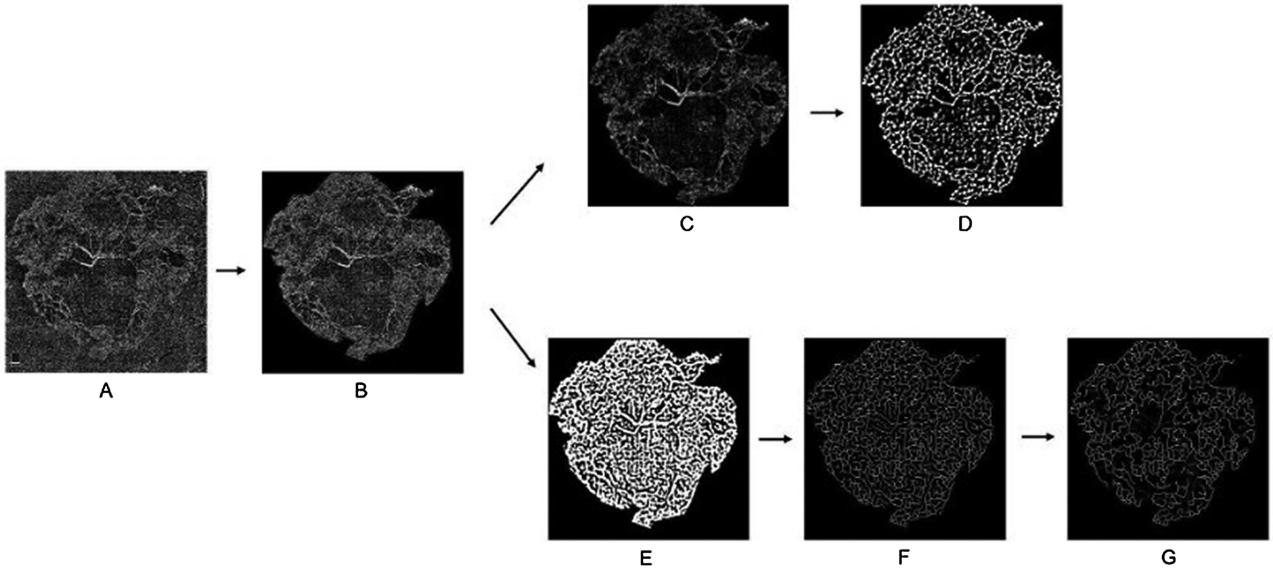

Figure 4. Intermediate stages of OCTA image processing analysis in a case of mature MNV. In the *upper row*, the image processing analysis, step by step, shows the preprocessing stage (**A**, **B**), the Gaussian blur filter (**C**), and the Frangi Vesselness (**D**) applications, whereas in the *bottom row* the application of the Mexican hat filter (**E**), the binary skeletonization (**F**) and the analysis of the skeleton image (**G**) are illustrated.

tonize the MNV image. After algorithm optimization with the Sauvola method for local adaptive thresholding (radius = 6) and successive white points measurement, VA and VD parameters were correct in all instances (100% rate). Finally, after refinement of the skeletonized image macro pathway, we were able to recognize the main trunk and correct vessel junctions number in 112 of the 127 scans (88.1% of cases).

The total runtime of the macro (excluding preprocessing) was 404.8 seconds (6 minutes and 44 seconds), with a mean of 3.2 ± 1.6 seconds per image. The 15 skeletonized images requiring manual reanalysis for correct branch and junction measurements, took a total of 555 seconds to be completed (37 seconds per image, on average).

Figures 3 and 4 show the intermediate stages of the algorithm pipeline in the analysis of a

structurally simpler and a more complex MNV, respectively.

Quantitative Results

Descriptive analysis of all OCTA biomarkers is presented in Table 1. Parameters including the means of MNV area (4.82 ± 4.81 mm^2), VA (1.79 ± 1.73 mm^2), total number of vascular junctions (135 ± 154), total number of branches (231 ± 257), and VL (40.5 ± 42.2 mm) exhibited a large standard deviation compared with their mean values, indicating a large amount of variation across different scans. By contrast, quantitative scores such as the means of FD (1.37 ± 0.08), VT (1.18 ± 0.06), VD (0.39 ± 0.04), and JD (3.19 ± 0.58 n/mm), showed low standard deviations, indicating that results were much more clustered around the central value. Finally, mean vessel diameter scores showed intermediate distribution features compared with the two aforementioned groups (46.9 ± 8.5 µm). Ten macro-computed OCTA biomarkers fell within the predicted value range obtained through manual methods. Comparison between low and high values of OCTA quantitative biomarkers is reported in Figure 5.

Influence of OCTA Biomarkers on Visual Acuity

Several clinical parameters significantly correlated with visual acuity. The correlation analysis showed a negative correlation of BCVA with MNV area (Spearman $\rho = -0.309$; $P = 0.002$), VA (Spearman $\rho = -0.315$; $P = 0.002$), total number of vascular junctions (Spearman $\rho = -0.285$; $P = 0.005$), and VL (Spearman $\rho = -0.304$; $P = 0.003$). The other parameters did not show a significant correlation with BCVA (Table 2).

Additionally, we split our sample into two groups based on visual results: eyes with BCVA equal to or less than 35 ETDRS letters (Snellen equivalent 20/200; $n =$ 72 eyes [57%]), and eyes with more than 35 ETDRS letters ($n = 55$ [43% of the cohort]). Binary logistic regression analysis findings for OCTA biomarkers associated with lower BCVA (≤35 letters) are summarized in Table 3. In the univariate analysis, only MNV area (odds ratio, 2.32) and total number of vascular junctions (odds ratio, 1.64) were significantly associated with lower BCVA ($P = 0.016$ and $P = 0.031$, respectively. FD showed a weak correlation with BCVA (odds ratio, 1.25; $P = 0.093$) that was not statistically significant (Fig. 6). VL ($P = 0.211$), VT ($P = 0.152$), VD ($P = 0.703$), and JD ($P = 0.871$) failed to correlate with BCVA.

Table 1. Descriptive Analysis of OCTA Biomarkers

	MNV Area (mm^2)	VA (mm^2)	Vessel Junctions (n)	Branches (n)	Average Length (mm)	Vessel Length (mm)	Fractal Dimension	Tortuosity	VD	JD (n/mm)	Vessel Diameter (µm)
Mean ± SD	4.82 ± 4.81	1.79 ± 1.73	135 ± 154	231 ± 257	0.19 ± 0.03	40.5 ± 42.2	1.37 ± 0.08	1.18 ± 0.06	0.39 ± 0.04	3.19 ± 0.58	46.9 ± 8.5
Median	3.05	1.21	82	140	0.18	26.1	1.38	1.16	0.38	3.16	44.8
Min	0.13	0.04	2	4	0.13	0.8	1.14	1.11	0.31	1.36	35.3
Max	24.15	8.86	935	1529	0.31	232.4	1.54	1.44	0.50	4.58	91.7

SD, standard deviation.

The table shows a descriptive analysis of all OCTA biomarkers derived from the macro applied to the 127-image dataset. Data are expressed as mean ± standard deviation. Median, minor, and maximum values were reported.

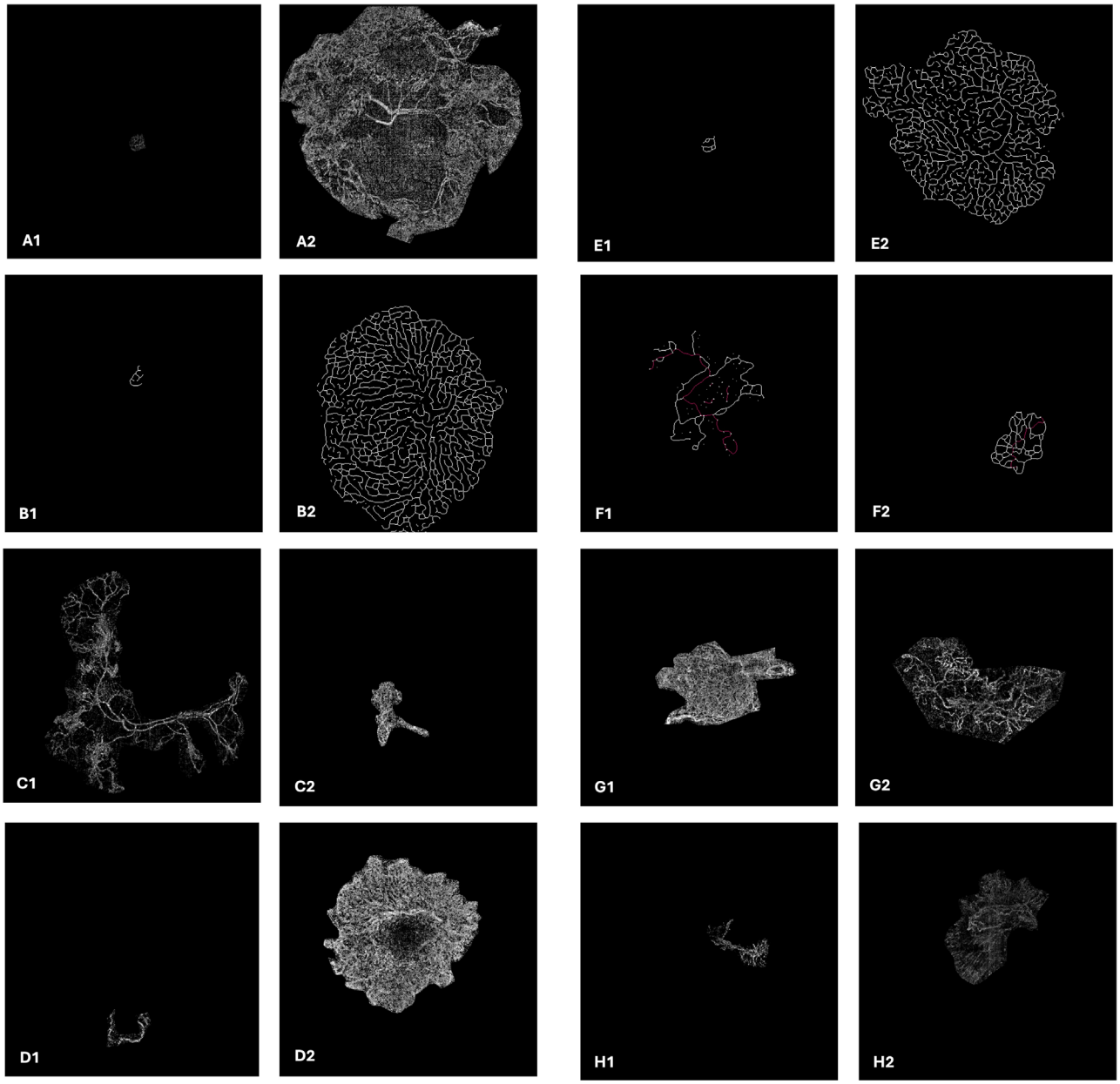

Figure 5. Comparison between low and high OCTA quantitative biomarkers. The composite showed the comparison between small (A1) and large (A2) MNV area, low (B1) and high (B2) total number of vascular junctions, low (C1) and high (C2) VD, low (D1) and high (D2) fractal dimension (FD), low (E1) and high (E2) vessel length (VL), low (F1) and high (F2) JD, low (G1) and high (G2) mean vessel diameter (MVD), and low (H1) and low (H2) VT.

Subgroup Analysis

Overall, the aforementioned three different morphological categories were distributed as follows: 11.8% of MNV lesions (15 eyes) showed an immature morphology, 17.3% of lesions (22 eyes) showed a mature morphology, and 70.9% of lesions (90 eyes) showed a hypermature morphology. In a post hoc analysis, the Tukey test was performed to assess the intergroup differences.

As illustrated in Figure 7, all structural parameters followed similar trends among the three groups, even if we did not report any statistically significant difference, owing to intergroup population disparity. When considering MNV area, VA, total number of vascular junctions, and VL, group 3 (hypermature morphology) showed higher values when compared with group 2 (mature morphology), which showed intermediate values, and group 1 (immature morphology), showed the lowest values for these parameters.

Table 2. Correlation Analysis Between OCTA Biomarkers and BCVA

Parameter	Spearman Rho	*P* Value
MNV area	−0.309	0.002
VA	−0.315	0.002
Vessel junctions	−0.285	0.005
Branches	−0.289	0.005
Average length	−0.052	0.621
Vessel length	−0.304	0.003
Fractal dimension	−0.071	0.494
Tortuosity	0.154	0.137
VD	0.023	0.827
JD	0.034	0.746
Vessel diameter	0.019	0.856

The correlation analysis showed a negative correlation between BCVA and MNV area, VA, vessel junctions, and vessel length. Other parameters did not show a significant correlation with BCVA.

Table 3. Association Between Quantitative Biomarkers and Low Visual Acuity

Predictor	*P* Value	OR	95% Confidence Interval
MNV area	0.016	2.3208	1.252–4.810
Vessel junctions	0.031	1.6376	1.303–1.973
Vessel length	0.211	0.7562	0.609–0.939
Fractal dimension	0.093	1.2510	1.015–1.404
Tortuosity	0.152	0.7749	0.544–0.989
VD	0.703	0.6612	0.358–1.003
JD	0.871	1.1052	0.330–3.703

OR, odds ratio.

Quantitative OCTA biomarkers associated with BCVA <35 ETDRS letters (Snellen equivalent 20/200) using Binary Logistic Regression Analysis.

Hosmer-Lemeshow test; test $\chi^2 = 3.305$, $P = 0.509$

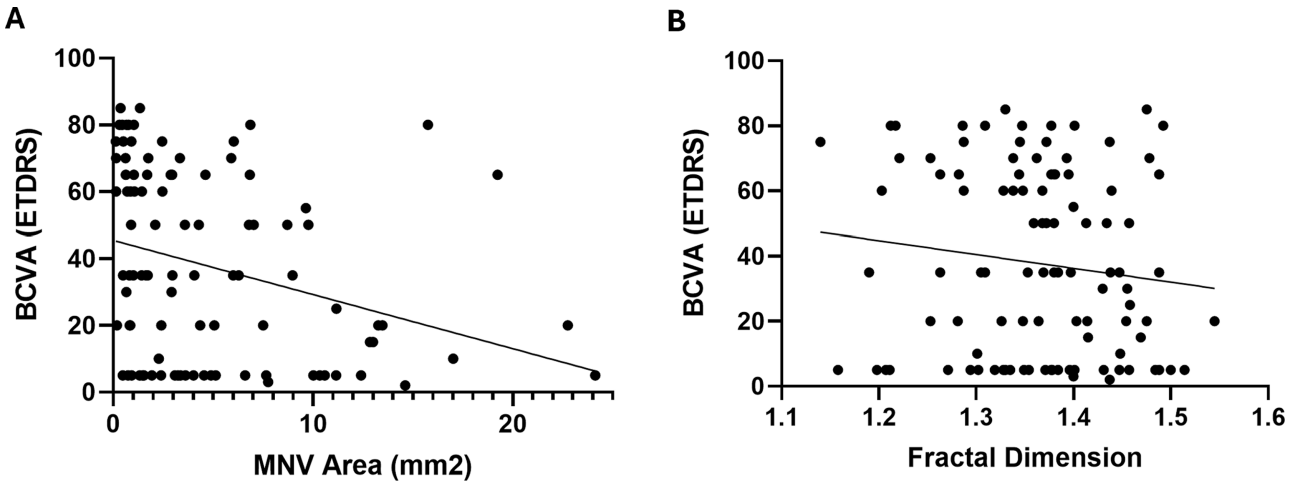

Figure 6. Linear regression correlating BCVA and MNV area and fractal dimension (FD). Simple linear regression graphs correlating BCVA with (A) MNV area and (B) FD, highlighting significant negative correlation for MNV area (slope −1.624; $R^2 = 0.088$; $P = 0.002$), while no significant correlation with fractal dimension (slope −42.36, $R^2 = 0.016$; $P = 0.20$).

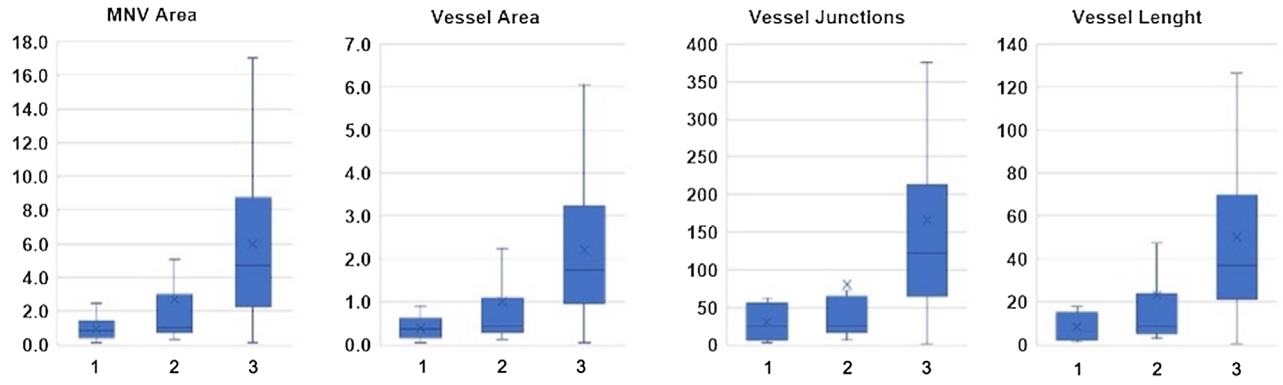

Figure 7. Subgroup analysis of structural MNV features. Line graphs show subgroup analysis of structural MNV features, such as MNV area, VA, and total number of vascular junctions and vessel length (VL), based on morphological aspect of the MNV: (1) immature group; (2) mature group; and (3) hypermature group.

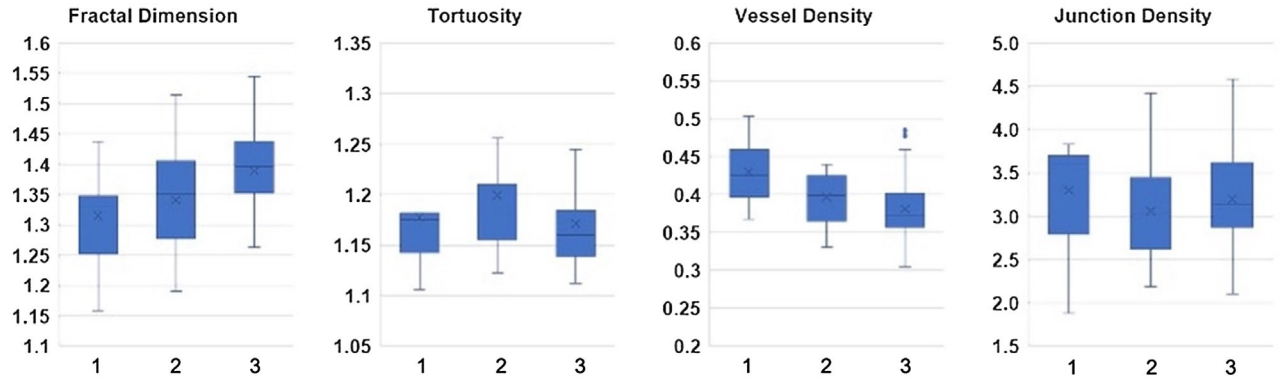

Figure 8. Subgroup analysis of mathematically derived MNV features. Line graphs show subgroup analysis of mathematically derived MNV features, including fractal dimension, tortuosity, VD and JD, based on morphological aspect of the MNV: (1) immature group; (2) mature group; and (3) hypermature group.

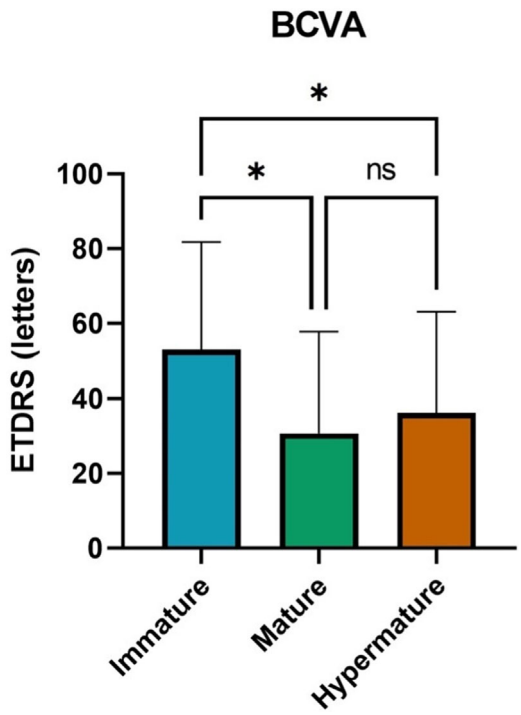

Figure 9. Ranks comparison analysis between BCVA and MNV morphology. The bar graph shows the mean BCVA difference between each morphological MNV subgroup (immature, mature, and hypermature MNV).

Referring to derived biomarkers (Fig. 8), FD showed similar trends, with the hypermature group illustrating higher values, whereas VD was higher in immature group and lower in the hypermature group.

Immature lesions were significantly associated with better visual acuity than mature and hypermature lesions. From the Kruskal-Wallis test, a mean difference of 21.9 letters ($P = 0.0338$) was noted between immature (mean BCVA 52.9 ± 28.9 [Snellen: 20/100]) and mature MNV (mean BCVA 30.7 ± 27.1 [Snellen: 20/250]). Comparing immature (mean BCVA 52.9 ± 28.9 [Snellen: 20/100]) and hypermature lesions (mean BCVA 36.2 ± 26.9 [Snellen: 20/200]), a mean difference 16.7 letters ($P = 0.0460$) was noted. Comparing mature (mean BCVA 30.7 ± 27.1 [Snellen: 20/250]) and hypermature MNVs (mean BCVA 36.2 ± 26.9 [Snellen: 20/200]), we found a mean difference of −5.2 letters ($P = 0.4932$). All data are summarized in Figure 9.

Discussion

OCTA enables a noninvasive detection and quantitative assessment of MNV and a detailed analysis of MNV morphological features. Although this capability has obvious diagnostic importance, especially because OCTA acquisition is fast and noninvasive, unlike dye-based angiography, the application of OCTA morphological biomarkers to gauge NV activity and guide anti-VEGF therapy is not yet a reliable practice.

The ImageJ macro tool developed in the current study applies a branching pipeline structure and improves the technique advanced by Wang et al.[12] by skeletonizing images using the Mexican Hat filter. Indeed, our system automatically calculated nine different biomarkers from OCTA image scans of MNV, including MNV area, total number of vascular junctions, VD, and FD.[12]

Our study demonstrated a negative correlation between MNV area and BCVA, which may be attributed to multiple factors associated with mature and hypermature lesions, including the longer duration of activity and the greater number of anti-VEGF injections associated with treatment of these lesions.

A negative correlation with BCVA was also observed for VA, total number of vascular junctions,

and VL, although only MNV area and vessel junction were associated with lower visual acuity (<35 letters) based on the binary logistic regression. As mentioned elsewhere in this article, all these parameters may be related to the longer course of disease associated with mature and hypermature MNV. Hypermature lesions, moreover, are typically characterized by greater outer retinal disorganization, fibrosis and atrophy, and lower visual acuity.[22] As expected, smaller lesions with immature morphological OCTA characteristics were associated with better BCVA, probably because the MNV is earlier in its growth course and less aggressive. Of note, JD cannot be considered as a consistent unique parameter, considering that a greater number of junctions can be seen in mature or hypermature MNVs, whereas more immature MNVs may show a remarkable lower number of junctions.

Our study is not the first investigation to use a semiautomatic analysis of MNV. Arrigo et al.[23–25] analyzed AMD-related MNV using binarization and skeletonization ImageJ filters and observed greater tortuosity in the vascular network in cases of active MNV associated with lower visual acuity outcomes. Further, MNV with lower VT at baseline was correlated with greater exudative activity but better visual outcome after intravitreal injections.[23–25] In another study however, MNV with higher VT was associated with less exudative activity and greater rates of atrophy and visual impairment.[26,27] In our analysis, we did not find a statistically significant correlation between VT and visual acuity or between VT and MNV morphology.

In a previous study, Coscas et al.[28] evaluated the blood flow area of active and fibrotic MNV, and the complexity and nonuniformity of the lesion through FD and lacunarity indexes, respectively. FD is a parameter describing the complexity of the vascular architecture and is expressed as a numerical value, which ranges between 0 and 2, derived from the number of the pixels representing the MNV.[22]

The Coscas group found a significant variability in lesion size that correlated with the activity of the MNV: Exudative lesions showed lower FD and lower median area than MNV in remission. Although no differences between active and fibrotic MNV were detected using lacunarity in the Coscas study, because of a lower branching complexity compared with inactive lesions, the FD showed lower values in eyes with active MNV. Accordingly, in our study we observed higher values of FD and MNV area in hypermature MNVs, although with no statistically significant difference between the three morphological subgroups, likely owing to the intergroup sample disparity.

A quantitative analysis of MNV using the ImageJ software was also performed by Al-Sheikh et al.[9] In contrast with our results as well as with those of Coscas et al., they did not detect any difference in MNV area in eyes with active lesions, that is, those under anti-VEGF treatment, vs. quiescent ones. Significantly lower FDs were instead detected in the quiescent group, supporting the already proposed hypothesis that hypermature MNV may be characterized by limited branching, straighter and longer vessels, and thus a less complex overall structure.[9,29] Faatz et al.,[22] who analyzed the NV changes in AMD eyes that had undergone anti-VEGF therapy, reported a significant decrease in the FD after the loading dose. The decrease in MNV complexity after the injections was associated with a marked decrease in vessel length. Indeed, peripheral capillaries are more susceptible to the effects of anti-VEGF drugs.[22,30,31] The greater variability in VL that we observed in our sample probably derived from the inclusion of MNV at different stages of disease.

Our results are aligned generally with those found in the previous literature, with some variability probably attributable to dataset differences.[11,12,32] We found that greater MNV area and complexity correlated with poorer visual acuity and that hypermature and mature lesions displayed the greatest area and complexity and immature lesions the least. This analysis only correlated OCTA morphological parameters with visual acuity outcomes and not with NV activity.

Our study has several limitations. One of the most important limitations is the inclusion of mainly advanced and treated MNV (mean of 18.4 previous anti-VEGFs injections). The other limitation was the inclusion of only type 1 MNV, the most common NV subtype. Furthermore, we did not perform a longitudinal study. Our study is cross-sectional. Additionally, we did not assess whether different anti-VEGF agents can be associated with a varying morphology of MNV, potentially leading to variations in morphological parameters. Because only one OCTA device was used to identify MNV, it is possible that outcomes may vary and influence the automated analysis according to the system used. However, the uniformity of the data acquisition can also be considered a strength of the study. Given the lower visual acuity of the recruited NV age-related macular degeneration patients in this study, imaging artifacts such as motion artifact can represent a significant challenge in the OCTA extraction and quantitative process.[33] However, we only included in our study those images with a quality index of greater than 7 out of 10 to decrease this risk. Last, artificial intelligence, which was not applied in our study, could provide more uniform outcomes. Further research is necessary to apply our algorithm to a larger cohort

of naïve lesions vs. those receiving anti-VEGF treatment and vs. those with inactive MNV, with the expectation that naïve lesions may be associated with a greater proportion of immature lesions providing more variability to the total cohort and potentially more valuable information.

Our findings represent a new step forward for the automated analysis of MNV associated with AMD, providing useful and practical tools for further research. OCTA analysis of MNV structure may predict visual acuity. The greater the MNV area and internal complexity, the lower the BCVA. Immature MNV correlated with better BCVA, whereas mature and hypermature lesions correlated with poorer visual acuity. Further studies are necessary to determine if classification of the morphology of MNV according to OCTA grading can predict visual acuity outcomes and activity of NV lesions and even guide anti-VEGF treatment.

Acknowledgments

The authors dedicate this paper to Bruno Lumbroso, our mentor and teacher, who devoted his life to the passionate study of retinal diseases, OCT, and OCTA, managing to instill in all of us a deep love for the same subjects. This is the last project to which Lumbroso contributed his invaluable expertise, and although he cannot witness its final realization, we are confident that he would be enthusiastic about it.

The authors also thank the Fondazione Policlinico Gemelli IRCCS and Italian Ministry of Health – Ricerca Corrente 2025.

Author Contributions: Data collection: C.F.; M.M.C.; I.B.; V.C., Writing paper: M.C.S.; C.F.; D.S. M.M.C; R.K., Idea of paper investigation: M.C.S., S.R., Review: M.C.S., C.F.; M.M.C., C.R., S.Z., F.F. D.S, S.R., Statistical Analysis: M.M.C., Critical revision: F.F.; S.R.; D.S., S.Z. D.M., All authors have read and agreed to the published version of the manuscript.

Data Statements: The data that support the findings of this study are available from the corresponding author, DS, upon reasonable request.

Disclosure: **M.C. Savastano**, None; **C. Fossataro**, None; **M.M. Carlà**, None; **V. Cestrone**, None; **I. Biagini**, None; **C. Rizzo**, None; **R. Kilian**, None; **S.A. Zweifel**, Alcon (C), Allergan (C), Apellis (C), Bayer (C), Endogena (C), Novartis (C), Roche (C), Bayer (F), Novartis (F); **D.R. Muth**, Roche (C); **F. Faraldi**, None; **S. Rizzo**, None; **D. Sarraf**, Amgen Inc. (C, F, R), Avecida (C), Boehringer Inc. (C, F), Eidon (P), Genentech, Inc. (C, F, R), Novartis Pharmaceuticals Corporation (C, S, R), Visionix/Optovue Inc. (C, F, S, I, P, R)

* MCS and CF contributed equally to the realization of the paper.

** SR and DS contributed equally to the revision of the paper.

References

1. Pugazhendhi A, Hubbell M, Jairam P, Ambati B. Neovascular macular degeneration: a review of etiology, risk factors, and recent advances in research and therapy. *Int J Mol Sci*. 2021;22(3):1170, doi:10.3390/ijms22031170.
2. Joachim N, Mitchell P, Burlutsky G, Kifley A, Wang JJ. The incidence and progression of age-related macular degeneration over 15 years: the blue mountains eye study. *Ophthalmology*. 2015; 122(12):2482–2489, doi:10.1016/j.ophtha.2015.08.002.
3. Buch H, Nielsen N V, Vinding T, Jensen GB, Prause JU, la Cour M. 14-year incidence, progression, and visual morbidity of age-related maculopathy: the copenhagen city eye study. *Ophthalmology*. 2005;112(5):787–798, doi:10.1016/j.ophtha.2004.11.040.
4. Savastano MC, Rispoli M, Lumbroso B, et al. Fluorescein angiography versus optical coherence tomography angiography: FA vs OCTA Italian study. *Eur J Ophthalmol*. 2021;31(2):514–520, doi:10.1177/1120672120909769.
5. Rispoli M, Savastano MC, Lumbroso B, Toto L, Di Antonio L. Type 1 choroidal neovascularization evolution by optical coherence tomography angiography: long-term follow-up. *Biomed Res Int*. 2020;2020:4501395, doi:10.1155/2020/4501395.
6. Malamos P, Tsolkas G, Kanakis M, et al. OCT-Angiography for monitoring and managing neovascular age-related macular degeneration. *Curr Eye Res*. 2017;42(12):1689–1697, doi:10.1080/02713683.2017.1356336.
7. Coscas F, Lupidi M, Boulet JF, et al. Optical coherence tomography angiography in exudative age-related macular degeneration: a predictive model for treatment decisions. *Br J Ophthalmol*. 2019;103(9):1342–1346, doi:10.1136/bjophthalmol-2018-313065.

8. Roberts PK, Nesper PL, Gill MK, Fawzi AA. Semiautomated quantitative approach to characterize treatment response in neovascular age-related macular degeneration: a real-world study. *Retina*. 2017;37(8):1492–1498, doi:10.1097/IAE.0000000000001400.
9. Al-Sheikh M, Iafe NA, Phasukkijwatana N, Sadda SR, Sarraf D. Biomarkers of neovascular activity in age-related macular degeneration using optical coherence tomography angiography. *Retina*. 2018;38(2):220–230, doi:10.1097/IAE.0000000000001628.
10. Cheng LN, Lin YX, Liu L, et al. Assessment of conbercept therapy for high myopia macular neovascularization by optical coherence tomography angiography. *Sci Rep*. 2020;10(1):16959, doi:10.1038/s41598-020-74073-1.
11. Choi M, Kim SW, Yun C, Oh J. OCT Angiography features of neovascularization as predictive factors for frequent recurrence in age-related macular degeneration. *Am J Ophthalmol*. 2020;213:109–119, doi:10.1016/j.ajo.2020.01.012.
12. Wang Y, Hu Z, Zhu T, et al. Optical coherence tomography angiography-based quantitative assessment of morphologic changes in active myopic choroidal neovascularization during anti-vascular endothelial growth factor therapy. *Front Med (Lausanne)*. 2021;8:657772, doi:10.3389/fmed.2021.657772.
13. Li S, Sun L, Zhao X, et al. Assessing the activity of myopic choroidal neovascularization: comparison between optical coherence tomography angiography and dye angiography. *Retina*. 2020;40(9):1757–1764, doi:10.1097/IAE.0000000000002650.
14. Daniel E, Toth CA, Grunwald JE, et al. Risk of scar in the comparison of age-related macular degeneration treatments trials. *Ophthalmology*. 2014;121(3):656–666, doi:10.1016/j.ophtha.2013.10.019.
15. Munk MR, Kashani AH, Tadayoni R, et al. Recommendations for OCT angiography reporting in retinal vascular disease: a Delphi approach by international experts. *Ophthalmol Retina*. 2022;6(9):753–761, doi:10.1016/j.oret.2022.02.007.
16. Xu D, Dávila JP, Rahimi M, et al. Long-term progression of type 1 neovascularization in age-related macular degeneration using optical coherence tomography angiography. *Am J Ophthalmol*. 2018;187:10–20, doi:10.1016/j.ajo.2017.12.005.
17. https://imagej.net/software/fiji/downloads.
18. Schürz M, Danmayr J, Jaritsch M, et al. EVAnalyzer: high content imaging for rigorous characterisation of single extracellular vesicles using standard laboratory equipment and a new open-source ImageJ/Fiji plugin. *J Extracell Vesicles*. 2022;11(12):e12282, doi:10.1002/jev2.12282.
19. Wu Y, Wang D, Wu X, et al. Optical coherence tomography angiography for the characterisation of retinal microvasculature alterations in pregnant patients with anaemia: a nested case–control study. *Br J Ophthalmol*. 2023;18(1):117–123. Published online November 25, 2022, doi:10.1136/bjo-2022-321781.
20. Deshpande A, Raman S, Dubey A, Susvar P, Raman R. An ImageJ macro tool for OCTA-based quantitative analysis of myopic choroidal neovascularization. *PLoS One*. 2023;18(4):e0283929, doi:10.1371/journal.pone.0283929.
21. Kalra G, Zarranz-Ventura J, Chahal R, Bernal-Morales C, Lupidi M, Chhablani J. Optical coherence tomography (OCT) angiolytics: a review of OCT angiography quantitative biomarkers. *Surv Ophthalmol*. 2022;67(4):1118–1134, doi:10.1016/j.survophthal.2021.11.002.
22. Faatz H, Rothaus K, Ziegler M, et al. The architecture of macular neovascularizations predicts treatment responses to anti-VEGF therapy in neovascular AMD. *Diagnostics*. 2022;12(11):2807, doi:10.3390/diagnostics12112807.
23. Arrigo A, Romano F, Aragona E, et al. Optical coherence tomography angiography can categorize different subgroups of choroidal neovascularization secondary to age-related macular degeneration. *Retina*. 2020;40(12):2263–2269, doi:10.1097/IAE.0000000000002775.
24. Arrigo A, Aragona E, Di Nunzio C, Bandello F, Parodi MB. Quantitative optical coherence tomography angiography parameters in type 1 macular neovascularization secondary to age-related macular degeneration. *Transl Vis Sci Technol*. 2020;9(9):48, doi:10.1167/tvst.9.9.48.
25. Arrigo A, Aragona E, Bordato A, et al. Quantitative optical coherence tomography angiography parameter variations after treatment of macular neovascularization secondary to age-related macular degeneration. *Retina*. 2021;41(7):1463–1469, doi:10.1097/IAE.0000000000003065.
26. Arrigo A, Aragona E, Bordato A, et al. Morphological and functional relationship between OCTA and FA/ICGA quantitative features in AMD-related macular neovascularization. *Front Med (Lausanne)*. 2021;8:758668, doi:10.3389/fmed.2021.758668.
27. Arrigo A, Bordato A, Aragona E, et al. Macular neovascularization in AMD, CSC and best vitelliform macular dystrophy: quantitative OCTA detects distinct clinical entities. *Eye*.

2021;35(12):3266–3276, doi:10.1038/s41433-021-01396-2.
28. Coscas F, Cabral D, Pereira T, et al. Quantitative optical coherence tomography angiography biomarkers for neovascular age-related macular degeneration in remission. *PLoS One*. 2018;13(10):e0205513, doi:10.1371/journal.pone.0205513.
29. Lumbroso B, Rispoli M, Savastano MC. Longitudinal optical coherence tomography–angiography study of type 2 naive choroidal neovascularization early response after treatment. *Retina*. 2015;35(11):2242–2251, doi:10.1097/IAE.0000000000000879.
30. Spaide RF. Optical coherence tomography angiography signs of vascular abnormalization with antiangiogenic therapy for choroidal neovascularization. *Am J Ophthalmol*. 2015;160(1):6–16, doi:10.1016/j.ajo.2015.04.012.
31. Kuehlewein L, Bansal M, Lenis TL, et al. Optical coherence tomography angiography of type 1 neovascularization in age-related macular degeneration. *Am J Ophthalmol*. 2015;160(4):739–48.e2, doi:10.1016/j.ajo.2015.06.030.
32. Deshpande A, Raman S, Dubey A, Susvar P, Raman R. An ImageJ macro tool for OCTA-based quantitative analysis of myopic choroidal neovascularization. *PLoS One*. 2023;18(4):e0283929, doi:10.1371/journal.pone.0283929.
33. Arrigo A, Aragona E, Battaglia Parodi M, Bandello F. Quantitative approaches in multimodal fundus imaging: state of the art and future perspectives. *Prog Retin Eye Res*. 2023;92:101111, doi:10.1016/j.preteyeres.2022.101111.